Dissipative dynamics of a system passing through a conical intersection: Ultrafast pump-probe observables

David Gelman[a)]
Fritz Haber Research Center for Molecular Dynamics, Hebrew University of Jerusalem, Jerusalem, 91904, Israel

Gil Katz[b)]
Department of Chemistry, Northwestern University, Evanston, Illinois 60208-3113

Ronnie Kosloff
Fritz Haber Research Center for Molecular Dynamics, Hebrew University of Jerusalem, Jerusalem, 91904, Israel

Mark A. Ratner
Department of Chemistry, Northwestern University, Evanston, Illinois 60208-3113

(Received 1 June 2005; accepted 18 July 2005; published online 6 October 2005)

The dynamics of a system incorporating a conical intersection, in the presence of a dissipative environment, is studied with the purpose of identifying observable ultrafast spectroscopic signatures. A model system consisting of two vibronically coupled electronic states with two nuclear degrees of freedom is constructed. Dissipation is treated by two different methods, Lindblad semigroup formalism and the surrogate Hamiltonian approach. Pump-probe experimental expectation values such as transient emission and transient absorption are calculated and compared to the adiabatic and diabatic population transfer. The ultrafast population transfer reflecting the conical intersection is not mirrored in transient absorption measurements such as the recovery of the bleach. Emission from the excited state can be suppressed on the ultrafast time scale, but the existence of a conical intersection is only one of the possible mechanisms that can provide ultrafast damping of emission. © *2005 American Institute of Physics*. [DOI: 10.1063/1.2032968]

I. INTRODUCTION

The Born–Oppenheimer[1] separation of nuclear and electronic motions is the enabler of nearly all our knowledge of molecular structure and dynamics. The adiabatic separation on which this principle is based, however, is never exactly correct, and there are instances where it fails substantially. The simplest example is probably nonradiative decay,[2] brought on by vibronic coupling.[3] In the standard Landau–Zener approach[4–7] motion along one coordinate modulates the nonadiabatic transition among electronic states. While the coupling is most easily envisaged along one coordinate, generalizing the Landau–Zener approach to multiple coordinates lies at the heart of contemporary models for electron transfer[8] and for nonradiative decay.[2]

Within the Landau–Zener picture, the nonadiabatic mixing is generally treated as a constant, invariant in the vibrational coordinates. More physically, this constant is sometimes modulated by a contour function (generally Gaussian), which limits the mixing to the region in which the different electronic potential energy surfaces come close to one another. More complicated nonadiabatic processes involve conical intersections.[9,10] These can exist in any dimensionality greater than one, so the simplest is the two-dimensional conical structure. Here the symmetry is such that the diabatic curves cross in an $(n-1)$ dimensional seam. In the adiabatic representation, the curves actually cross at a single point, because of the symmetry (odd in one of the coordinates) of the vibronic coupling. More complicated structures (higher-dimensional conical intersections, asymmetric conical intersections, pairs or clusters of conical intersections) can also occur. They are common for larger organic molecules,[11–13] and they offer complex higher-order mixing patterns in the dynamics.

Because of the different geometry of curve crossing between isolated Landau–Zener-avoided crossings and higher-dimensional conical intersections, population transfer can be very rapid in the conical case. This is what led to the original interest in conical intersections, and it has been extensively discussed, particularly using density operator methods.[14–18] The organic literature[12,19] broadly uses conical intersections to discuss subpicosecond transitions. There is extensive and elegant analyses, including simulations, more formal analyses, and careful experimental comparisons.

In this paper, we focus on decay of photoexcited states, and on the experimental observables of luminescence, pump-probe spectra, and recovery of the bleach. All of these are governed not only by the population dynamics, but also by the value of the transition dipole moment and by energy redistribution. Hence it is necessary to deal not only with the electronic state population, but also with the energy distribution. In nearly all cases, then, we have in addition to the curve crossing problem an intramolecular vibrational relax-

[a)]Electronic mail: davg@fh.huji.ac.il
[b)]Electronic mail: gkatz@chem.northwestern.edu

ation (IVR) issue—the system must return to the starting configuration for bleach recovery to be observed, and back transfer (recrossing) can occur in the excited state unless either IVR or effective dephasing make such recurrences impossible.

Most theoretical analyses of conical intersections uses either two or three nuclear modes.[14] Electron populations can then indeed describe ultrafast behavior returning to the ground electronic state, and some aspects of IVR and phase loss can also be understood. But the fundamental behavior of conical intersections in molecules larger than triatomic arises from the presence of multiple modes, and explicit treatment of multiple modes remains difficult. There is an exemplary analysis of a 24-mode dynamics model for pyrazine,[20] as well as calculations utilizing a Redfield[21,22] approach to deal with the rest of the vibrational modes as comprising a harmonic bath.[23,24]

In this paper, we use a direct propagation scheme to examine a two-mode model for conical intersections. The aim is to investigate both population dynamics and bleach recovery, in order to relate them to experimental observations. Since the direct propagation of such a system scales exponentially with the number of modes, we use a system-bath approach, with two active vibrational modes and two electronic states chosen as the system, and a representation of the bath. We use two different treatments of this bath: first, a reduced description based on a density operator treatment where the dynamics is generated by the Lindblad formalism of semigroup dynamics;[25–27] alternatively, we use a wave-function propagation scheme with the so-called surrogate Hamiltonian[28] method, corresponding to an Ohmic distribution of spin modes in the bath. The focus is on photochemical dynamics, and the photochemical excitation is treated nonperturbatively—a system-electromagnetic field determination is included in the time-dependent Hamiltonian. For clarity, all the calculations are carried out in the diabatic representation.

Using this bath model, while the population transfer is indeed in the subpicosecond regime, the bleach recovery is dominated by subsequent dephasing and IVR, and therefore can proceed far more slowly. While the two-dimensional coupling scheme can mix states very rapidly, it cannot by itself (in the absence of ultrafast IVR or dephasing) lead to the fast bleach recovery. These observations have several implications: they suggest, for example, that the occurrences of 100 fs time-scale bleach recovery in transition metal complexes in solution[29–31] might be better explained by simple avoided crossings with strong outer sphere reorganization coupling terms than by invoking a conical intersection. They also suggest that conical mixing symmetry is not itself sufficient to generate femtosecond bleach recovery or relaxation.

The article is organized as follows. Section II A outlines the formal structure of the model, Sec. II B reviews the surrogate Hamiltonian approach, while the semigroup method is described in Sec. II C. The connection to observables is discussed in Sec. II D. Actual results are presented in Sec. III, and some remarks are made in the concluding section.

II. THEORY

A. The model

The study of dissipative effects on nonadiabatic dynamics of multidimensional systems is not a trivial task. The main obstacle in modeling such systems is rooted in the exponential growth in complexity with the number of degrees of freedom. Significant simplifications can be achieved by partitioning the total system into a primary part and a bath describing the environment.[32] The Hamiltonian of such a combined system is given by

$$\hat{\mathbf{H}} = \hat{\mathbf{H}}_{\mathrm{S}} \otimes \mathbb{1}_{\mathrm{B}} + \mathbb{1}_{\mathrm{S}} \otimes \hat{\mathbf{H}}_{\mathrm{B}} + \hat{\mathbf{H}}_{\mathrm{SB}} + \hat{\mathbf{H}}_{\mathrm{SF}}(t), \tag{1}$$

where $\hat{\mathbf{H}}_{\mathrm{S}}$ is the Hamiltonian of the primary system, $\hat{\mathbf{H}}_{\mathrm{B}}$ is the bath Hamiltonian, and $\hat{\mathbf{H}}_{\mathrm{SB}}$ describes the interaction between the system and the bath. The time-dependent interaction of the system with the external electromagnetic field is represented by $\hat{\mathbf{H}}_{\mathrm{SF}}(t)$.

The primary system usually consists of a few physically relevant degrees of freedom, which are treated explicitly. The bath, on the other hand, consists of an infinite number degrees of freedom and enters the model implicitly, i.e., only its influence on the primary system is important. In the context of conical intersections, the bath may describe a condensed-phase environment, as well as the molecule's inactive modes.

Let us consider the simplest model of a symmetry-allowed conical intersection.[9,10,33] It includes two electronic states g and e, and two vibrational modes: the totally symmetric Q_0 (also called the tuning mode), and the symmetry-breaking (coupling) mode Q_c, which is responsible for vibronic coupling.[15] Employing a diabatic electronic representation, the system Hamiltonian can be written as

$$\hat{\mathbf{H}}_{\mathrm{S}} = \begin{pmatrix} \hat{\mathbf{H}}_{\mathrm{g}} & V_{\mathrm{d}}(\hat{\mathbf{Q}}_c) \\ V_{\mathrm{d}}(\hat{\mathbf{Q}}_c) & \hat{\mathbf{H}}_{\mathrm{e}} \end{pmatrix} \otimes \mathbb{1}_{\mathrm{B}}, \tag{2}$$

with $\hat{\mathbf{H}}_{\mathrm{g/e}} = \hat{\mathbf{T}} + V_{\mathrm{g/e}}(\hat{\mathbf{Q}}, \hat{\mathbf{Q}}_c)$. $\hat{\mathbf{T}}$ is the kinetic energy operator, V_{g} and V_{e} are the potential energy operators on the ground and excited electronic states, respectively, and V_{d} is the diabatic coupling. The $\hat{\mathbf{Q}}_c$, $\hat{\mathbf{Q}}_0$ are chosen to be dimensionless.

It is customary to choose a linear form for the diabatic coupling term:

$$V_{\mathrm{d}}(\hat{\mathbf{Q}}_0, \hat{\mathbf{Q}}_c) = \Lambda \hat{\mathbf{Q}}_c, \tag{3}$$

which is appropriate in the vicinity of the conical intersection. Since diabatic coupling functions obtained from *ab initio* calculations turn out to be localized,[34,35] the more physically motivated choice is a coupling term modulated by a damping Gaussian:

$$V_{\mathrm{d}}(\hat{\mathbf{Q}}_0, \hat{\mathbf{Q}}_c) = \Lambda \hat{\mathbf{Q}}_c e^{-(\hat{\mathbf{Q}}_0 - Q_{\mathrm{CI}})^2/\sigma^2 - \hat{\mathbf{Q}}_c^2/\sigma^2}, \tag{4}$$

where Q_{CI} is the point at which the conical intersection occurs along the symmetric mode Q_0. Thus the diabatic coupling is damped out as one moves away from the conical intersection point.[36,37] Complications will arise if the conical intersection is close to the Franck–Condon region, which will lead to interferences with the light induced excitation

dynamics. This possibility will be excluded in the present study.

The coupling with the radiation is described by the semiclassical time-dependent Hamiltonian

$$\hat{\mathbf{H}}_{\mathrm{SF}} = \begin{pmatrix} 0 & -\epsilon(t)\hat{\boldsymbol{\mu}}_{\mathrm{tr}} \\ -\epsilon^{*}(t)\hat{\boldsymbol{\mu}}_{\mathrm{tr}} & 0 \end{pmatrix} \otimes \mathbb{1}_{\mathrm{B}}, \tag{5}$$

where $\hat{\boldsymbol{\mu}}_{\mathrm{tr}} = \hat{\boldsymbol{\mu}}_{\mathrm{tr}}(\hat{\mathbf{Q}}_0, \hat{\mathbf{Q}}_c)$ is the electronic transition dipole operator, which is a function of the nuclear configuration. $\epsilon(t)$ is the time-dependent electric field. In the large wavelength limit the spatial dependence of $\epsilon(t)$ is ignored.

B. The surrogate Hamiltonian

The surrogate Hamiltonian method[28] is based on the idea that for sufficiently short times the system is not able to resolve the full density of the bath states. Therefore it is possible to replace an infinite number of the bath modes by a finite set of representative modes. This new "surrogate" Hamiltonian faithfully represents the dynamics of the primary system under the influence of an infinite bath for a *finite* time.

The starting point is to decompose the bath into a sum of single mode Hamiltonians $\hat{\mathbf{h}}_i$:

$$\hat{\mathbf{H}}_{\mathrm{B}} = \sum_{i}^{N} \hat{\mathbf{h}}_i \tag{6}$$

For the surrogate Hamiltonian a bath of two-level systems (TLS) is employed:

$$\hat{\mathbf{h}}_i = \hbar\omega_i \hat{\boldsymbol{\sigma}}_i^{\dagger} \hat{\boldsymbol{\sigma}}_i, \tag{7}$$

where $\hat{\boldsymbol{\sigma}}_i^{\dagger}$, $\hat{\boldsymbol{\sigma}}_i$ are the standard spin creation and annihilation operators of mode i with gap ω_i.

The interaction between system and bath is described by the Hamiltonian $\hat{\mathbf{H}}_{\mathrm{SB}}$, which can be decomposed into a sum of products of system and bath operators without loss of generality. The system-bath interaction $\hat{\mathbf{H}}_{\mathrm{SB}}$ can be partitioned into terms describing different physical processes. The most general bilinear form for vibrational relaxation is given by the operator

$$\hat{\mathbf{H}}_{\mathrm{SB}}^{vr} = \begin{pmatrix} f_{\mathrm{g}}(\hat{\mathbf{Q}}_0, \hat{\mathbf{Q}}_c) & 0 \\ 0 & f_{\mathrm{e}}(\hat{\mathbf{Q}}_0, \hat{\mathbf{Q}}_c) \end{pmatrix} \otimes \sum_{\alpha=0,c} \sum_{i}^{N} \lambda_i^{\alpha} (\hat{\boldsymbol{\sigma}}_i^{\alpha\dagger} + \hat{\boldsymbol{\sigma}}_i^{\alpha}), \tag{8}$$

where $f(\hat{\mathbf{Q}}_0, \hat{\mathbf{Q}}_c)$ is a function of the system coordinate(s) operator. The system-bath coupling can vary between the ground and the excited potentials.

In the weak system-bath coupling regime the influence of the bath on the primary system is fully characterized by the spectral density function $J(\omega)$:[32]

$$J(\omega) = \sum_{i} |\lambda_i|^2 \delta(\omega - \omega_i). \tag{9}$$

Use of the density of states $\rho(\omega_i) = (\omega_{i+1} - \omega_i)^{-1}$ in place of the delta function in Eq. (9) determines the coupling constants:[38,39]

$$\lambda_i = \sqrt{J(\omega_i)/\rho(\omega_i)}. \tag{10}$$

The sampling density in energy of this set is determined by the inverse of the time interval. The finite bath of N spins is constructed with a system-bath coupling term, which in the limit $N \to \infty$ converges to the given spectral density of the full bath. The surrogate Hamiltonian, consists of a finite number of bath modes, and it is therefore limited to representing the dynamics of the investigated system for a finite time (shorter than the Poincaré period at which recurrences appear[40]). These recurrences are caused by the finite size of the bath so that after some time the energy flow into the bath partly is reversed.

Within the surrogate Hamiltonian method, it is straightforward to introduce into the model different system-bath interaction mechanisms, such as electronic and vibrational pure dephasing. The process of dephasing corresponds physically to fluctuations in the values of the system energies—electronic dephasing is then the fluctuation in the electronic energy levels, while vibrational dephasing describes changes in the vibrational energies. A qualitative picture of pure dephasing is based on an almost elastic exchange of energy between bath modes, which alters the accumulated phase of the system. For electronic dephasing, the bath modulates the electronic excitation:

$$\hat{\mathbf{H}}_{\mathrm{SB}}^{\mathrm{ed}} = \Delta_V(\hat{\mathbf{Q}}_0, \hat{\mathbf{Q}}_c) \frac{1}{2} \begin{pmatrix} -1 & 0 \\ 0 & 1 \end{pmatrix} \otimes \sum_{ij} c_{ij}^{\mathrm{ed}} (\hat{\boldsymbol{\sigma}}_i^{\dagger} \hat{\boldsymbol{\sigma}}_j + \hat{\boldsymbol{\sigma}}_j^{\dagger} \hat{\boldsymbol{\sigma}}_i). \tag{11}$$

$\Delta_V(\hat{\mathbf{Q}}_0, \hat{\mathbf{Q}}_c)$ is the difference potential describing the dependence of the modulation on the nuclear displacement. The coefficients c_{ij} are biased to represent almost elastic encounters,

$$c_{ij} = \bar{c}_e e^{-(\omega_i - \omega_j)^2/2\sigma_\omega^2}, \tag{12}$$

with $\bar{c}_e$ a global dephasing parameter, and σ_ω determines the inelastic width. The dephasing rate is proportional to the square of the band width of c_{ij}.[36]

For vibrational dephasing, the bath modulates the vibrational Hamiltonian:

$$\hat{\mathbf{H}}_{\mathrm{SB}}^{\mathrm{vd}} = \begin{pmatrix} \hat{\mathbf{H}}_g & 0 \\ 0 & \hat{\mathbf{H}}_e \end{pmatrix} \otimes \sum_{ij} c_{ij}^{\mathrm{vd}} (\hat{\boldsymbol{\sigma}}_i^{\dagger} \hat{\boldsymbol{\sigma}}_j + \hat{\boldsymbol{\sigma}}_j^{\dagger} \hat{\boldsymbol{\sigma}}_i). \tag{13}$$

In order to activate a pure dephasing process, the bath modes must be initially populated. The detailed algorithm of applying Eqs. (11)–(13) has been described in Ref. 36.

The full surrogate Hamiltonian contains all possible correlations between the primary system and the environment. The combined system-bath state is described by a 2^N-dimensional spinor with N being the number of bath modes. The spinor is bit ordered, i.e., the jth bit set in the spinor index corresponds to the jth TLS mode, which is excited if the counting of bits starts at $j=0$. The dimension 2^N results from the total number of possibilities to combine two states N times.

In the weak coupling limit considering all 2^N possibilities of combining the bath modes might not be necessary. Thus for short time dynamics, it is possible to restrict the number of simultaneous bath excitations.[41,42]

The spin bath employed by the surrogate Hamiltonian has its origin in a tight binding model of condensed phase. It represents in general a different physical model than the widely used model bath of noninteracting harmonic oscillators. However, a recently performed comparison[42] has shown that the dynamics induced by two baths (even in the strong coupling limit) are very similar.

Observables associated with operators of the primary system are determined from the reduced system density operator: $\hat{\boldsymbol{\rho}}_S(Q,Q')=\mathrm{tr}_B\{|\Psi\rangle\langle\Psi|\}$, where $\mathrm{tr}_B\{\}$ is a partial trace over the bath degrees of freedom. The system density operator is constructed from the total system-bath wave function and only this function is propagated. A grid representation is used to represent each spinor component of the wave function. The kinetic energy operator is applied in Fourier space employing fast Fourier transform,[43] and the Chebychev method[44,45] is used to compute the evolution operator. Numerical details for applying the bath operators have been described in Refs. 28 and 36.

C. Reduced dynamics in the density operator representation

The reduced dynamics approach is constructed to avoid the size scaling of a full treatment, allowing a computational scheme able to simulate a dynamical encounter from first principles. The equations of motion are solved explicitly for a primary system, while the bath is treated implicitly. The approach requires equations of motion for the subsystem which are based on Lindblad formalism of semigroup dynamics.[25–27] One advantage of the semigroup approach is that the computational cost scales linearly with the propagation time, unlike the exponential scaling of the surrogate Hamiltonian. A disadvantage is that it is formulated in Liouville space, which squares the number of required representation points in comparison to a wave function description of the surrogate Hamiltonian method. In addition, there is a hidden assumption[46] of an uncorrelated initial state of the system and the bath. One starting point is to formulate the time evolution equations as an integrodifferential equation:[47,48]

$$\frac{d}{dt}\hat{\boldsymbol{\rho}}_S=\mathcal{L}_S(\hat{\boldsymbol{\rho}}_S)+\int^t \mathcal{K}(t,\tau)\hat{\boldsymbol{\rho}}_S(\tau)d\tau, \tag{14}$$

where $\mathcal{L}_S$ is the system's free Liouville operator and $\mathcal{K}$ is a memory kernel which includes implicitly the bath dynamics. A key ingredient in the formulation is that the combined system-bath dynamics is generated by a unitary evolution $\hat{\boldsymbol{\rho}}(t)=\mathrm{tr}\{\hat{\mathbf{U}}(t)\hat{\boldsymbol{\rho}}_S(0)\otimes\hat{\boldsymbol{\rho}}_B(0)\hat{\mathbf{U}}^\dagger(t)\}$. Such a construction leads to formal restriction on the subsystem equation of motion known as complete positivity,[49] meaning physically, that no populations (of the combined system and bath) should be negative. In the Markovian limit, under the conditions of the complete positivity, the reduced equation of motion can be diagonalized to the Lindblad form:

$$\frac{d}{dt}\hat{\boldsymbol{\rho}}_S=-\frac{i}{\hbar}[\hat{\mathbf{H}}_S,\hat{\boldsymbol{\rho}}_S]+\sum_j\left(\hat{\mathbf{F}}_j\hat{\boldsymbol{\rho}}_S\hat{\mathbf{F}}_j^\dagger-\frac{1}{2}\{\hat{\mathbf{F}}_j\hat{\mathbf{F}}_j^\dagger,\hat{\boldsymbol{\rho}}_S\}\right), \tag{15}$$

where $\hat{\mathbf{F}}_j$ are the Lindblad operators, representing the influence of the environment. $\{\hat{\mathbf{A}},\hat{\mathbf{B}}\}=\hat{\mathbf{A}}\hat{\mathbf{B}}+\hat{\mathbf{B}}\hat{\mathbf{A}}$ is the anticommutator.

The nature of the bath is implied in the formulation of a specific Lindblad operator. Such operators can be constructed to display vibrational and electronic dissipation[50,51] of the system in baths of different physical natures. The rate of dissipation is derived from the nature of the bath and the system-bath coupling.

The choice $\hat{\mathbf{F}}_{vd}=(\sqrt{\gamma_{vd}}\phi/\hbar)\hat{\mathbf{H}}$ dictates pure vibrational dephasing of the system (γ_{vd} is the rate and ϕ is the phase shift in time). $\hat{\mathbf{F}}_{ed}=\sqrt{\gamma_{ed}}(|e\rangle\langle e|-|g\rangle\langle g|)$ represents electronic dephasing.[50,52] For physical reasons we chose the electronic dephasing operator to be in the diabatic representation. The reason is that the major interaction with the environment is induced by the transition dipole of the molecule, proportional to $(|e\rangle\langle e|-|g\rangle\langle g|)$ in the Condon approximation and the diabatic representation.

Quantum intramolecular vibrational relaxation is achieved using equations of motion,[53,54] which are consistent with complete positivity:

$$\frac{d}{dt}\hat{\boldsymbol{\rho}}_S=-\frac{i}{\hbar}[\hat{\mathbf{H}},\hat{\boldsymbol{\rho}}_S]-\frac{i}{2\hbar}\gamma[\hat{\mathbf{q}},\{\hat{\mathbf{p}},\hat{\boldsymbol{\rho}}_S\}]-\frac{1}{\hbar^2}D_{pp}[\hat{\mathbf{q}},[\hat{\mathbf{q}},\hat{\boldsymbol{\rho}}_S]]$$
$$-\frac{1}{\hbar^2}D_{qq}[\hat{\mathbf{p}},[\hat{\mathbf{p}},\hat{\boldsymbol{\rho}}_S]]-\frac{2}{\hbar^2}D_{pq}[\hat{\mathbf{q}},[\hat{\mathbf{p}},\hat{\boldsymbol{\rho}}_S]], \tag{16}$$

where thermal equilibrium imposes $D_{pp}=\gamma m k_b T$ and $D_{qq}=\kappa(\gamma\hbar^2/16mk_bT)$. p and q are momentum and space variables of the system. The κ is a parameter larger than 1 (for $\kappa=4/3$ the model is Gaussian, and if κ is larger, the model is Poisson-like). A cross diffusion term can be added: $D_{pq}=\gamma\Omega\hbar^2/12\pi k_bT$, where Ω is the frequency cutoff parameter.

It should be noticed that D_{ij} terms are independent of the field.

D. Stimulation of pump-probe experiment and time-dependent observables

From the experimental point of view, the detection of ultrafast nonadiabatic processes becomes possible using femtosecond pump-probe techniques.[29,30,55–59] These experiments provide information on the time scales of the processes under investigation. Nevertheless, the interpretation of the results remains a nontrivial task. A direct signature of the ultrafast dynamics in such experiments are transient modulations of optical observables, reflecting the promotion of ground and excited state vibrational modes. However, it is generally not possible to define the exact number of electronic states and vibrational modes involved in the nonadiabatic dynamics.

The present study aims to construct a simplified quantum dynamical model, including a conical intersection, and to apply the previously developed tools[36,60,61] to simulate the pump-probe experiments.

The surrogate Hamiltonian simulations start with a fully correlated ground state, determined by propagating an initial guess function in imaginary time[44] with the total system-bath Hamiltonian:

$$\Psi(\hat{\mathbf{Q}};\tau) = e^{-\hat{\mathbf{H}}\tau}\Psi(\hat{\mathbf{Q}};0). \tag{17}$$

This initial state is the starting point for launching the pump-probe simulations. The use of the surrogate Hamiltonian has the advantage of a consistent treatment of initial correlations between the system and the bath, as well as explicit description of the pulse field and its influence on the system-bath interactions. Commonly in most computational studies of nonadiabatic processes, the initial state is prepared by a Franck–Condon transition from the ground state.[14] This choice, however, ignores the system-bath correlations and the dynamical aspects of the pump pulse.

Upon applying the pump pulse, a significant fraction of the population is transferred to the excited state. Since the pump pulse is strong, a nonperturbative treatment is needed. Our model enables us to include explicitly the interaction between the system and the radiation (5). In this study the pump pulse has a Gaussian envelope in time:

$$\epsilon(t) = \epsilon_0 e^{-(t-t_{\max})^2/2\sigma_L^2} e^{i\omega_L t}, \tag{18}$$

and the carrier frequency ω_L is chosen to match the difference between the ground and excited electronic potentials at the minimum of the ground state.

The probe pulse can be applied at any stage in the cycle of events. Typically, the probe pulse is short and weak. It can promote both, excitation, leading to the energy absorption, and deexcitation, resulting in stimulated emission. In this case a perturbative picture is justified and can save a significant computational effort. The total absorption from the probe pulse by an observable is thus represented by a window operator $\hat{\mathbf{W}}$. This operator describes a finite resolution position measurement:[60,62]

$$\Delta E \approx -\hbar\omega_L \mathrm{tr}_S\{\hat{\boldsymbol{\rho}}_S(t_p)\cdot\hat{\mathbf{W}}\}. \tag{19}$$

The observation process is completed in a time duration proportional to the probe pulse duration τ_p. Equation (19) collapses the observation to a single instant of time t_p. By employing time-dependent perturbation theory the window operator for a Gaussian-shaped probe pulse becomes[60,62]

$$\hat{\mathbf{W}}(\hat{\mathbf{Q}},\hat{\mathbf{Q}}') = \frac{\pi(\tau_p^2\epsilon_0^2)}{\hbar^2} e^{-2\Delta(\hat{\mathbf{Q}})^2\tau_p^2/\hbar^2}\cdot\hat{\boldsymbol{\mu}}^2(\hat{\mathbf{Q}}) \times \delta(\hat{\mathbf{Q}}-\hat{\mathbf{Q}}')|\psi_k\rangle\langle\psi_k|, \tag{20}$$

where $|\psi_k\rangle\langle\psi_k|$ is the electronic projection operator, which selects the ground electronic state for transient absorption. For emission, the projection operator selects the excited electronic state. The window operator, Eq. (20), is a function of the probe central frequency ω_L:

$$2\Delta(\hat{\mathbf{Q}}) = V_e(\hat{\mathbf{Q}}) - V_g(\hat{\mathbf{Q}}) - \hbar\omega_L, \tag{21}$$

i.e., $2\Delta(\hat{\mathbf{Q}})$ is the difference potential relative to the probe frequency. The employment of the window operator assumes a random phase between the pump and probe pulses, eliminating interference effects. An interference between pump and probe excitations is also eliminated once the electronic dephasing is complete. The memory of the pump phase is stored in the transition dipole phase. This is erased once the relative phase between the ground and excited wave packets is lost by the electronic dephasing.[63]

The present modeling of the pump-probe experiment enables us to investigate the population dynamics, as well as the energy distribution during the nonadiabatic dynamics. The dynamics of the excited electronic state is reflected in the stimulated-emission signal. The vibrational relaxation of the hot ground state population, on the other hand, cannot be monitored by the time evolution of the vibrational population or the stimulated emission. The transient absorption, however, reflects the energy redistribution, since it shows the returning of the system to its initial configuration. The ground-state absorption bleaching, induced by the pump probe, will exhibit the recovery, reflecting the curve crossing dynamics as well as the subsequent vibrational cooling.

Most studies of nonadiabatic processes involving conical intersections consider the overall electronic populations of the excited and the ground electronic states.[14,15,64,65] In the case of open-system dynamics, the time-dependent population probabilities of the diabatic electronic states are defined as

$$P_n^{di}(t) = \mathrm{tr}\{\hat{\mathbf{N}}_n^{di}\hat{\boldsymbol{\rho}}_S(t)\}, \tag{22}$$

with $\hat{\mathbf{N}}_n^{di}$ being the projection operator of the nth electronic state in the diabatic representation. The reduced system density operator is defined as a partial trace over the bath degrees of freedom. The adiabatic electronic population is defined in a similar way by using diabatic-to-adiabatic transformation.[15]

A question that naturally arises is how the population dynamics is monitored experimentally. This has been the leading argument in studies modeling femtosecond time-resolved experiments in systems incorporating conical intersections.[66,67]

III. RESULTS AND DISCUSSION

A. General

The diabatic potential energy surfaces are approximated by quadratic functions with linear intrastate couplings.[15] Using dimensionless normal coordinates,

$$V_g(\hat{\mathbf{Q}}_0,\hat{\mathbf{Q}}_c) = -\Delta_0 + \frac{\hbar\omega_0}{2}\hat{\mathbf{Q}}_0^2 + \kappa_g\hat{\mathbf{Q}}_0 + \frac{\hbar\omega_c}{2}\hat{\mathbf{Q}}_c^2, \tag{23}$$

$$V_e(\hat{\mathbf{Q}}_0,\hat{\mathbf{Q}}_c) = \Delta_0 + \frac{\hbar\omega_0}{2}\hat{\mathbf{Q}}_0^2 + \kappa_e\hat{\mathbf{Q}}_0 + \frac{\hbar\omega_c}{2}\hat{\mathbf{Q}}_c^2, \tag{24}$$

where ω_0 and ω_c are the vibrational frequencies of the totally symmetric mode Q_0 and the coupling mode Q_c respectively. The $2\Delta_0$ denotes the vertical excitation energy and $\kappa_{g/e}$ are the first-order intrastate electron-vibrational couplings.

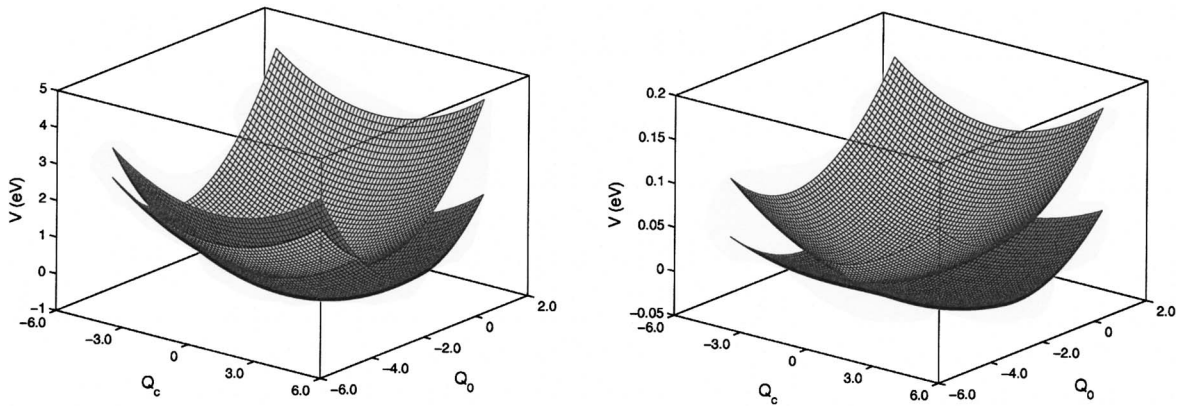

FIG. 1. Schematic view of the potential energy surfaces in a diabatic (upper panel) and an adiabatic (lower panel) representation. The following parameters are used in the calculations (all in eV): $\omega=0.074$, $\omega_c=0.0936$, $\kappa_g=-0.0964$, $\kappa_e=0.1194$, $\Lambda=0.18$ $\Delta=0.4617$ and the coordinates are dimensionless.

The system parameters are chosen as follows (all in eV): $\omega_0=0.074$, $\omega_c=0.0936$, $\kappa_g=-0.0964$, $\kappa_e=0.1194$, $\Delta=0.4617$ and the coordinates are dimensionless. The interstate coupling is described as

$$V_{\mathrm{d}}(\hat{\mathbf{Q}}_0,\hat{\mathbf{Q}}_c)=\Lambda\hat{\mathbf{Q}}_c e^{-(\hat{\mathbf{Q}}_0-Q_{\mathrm{CI}})^2/2\sigma^2}, \tag{25}$$

with Q_{CI} being the point where the conical intersection occurs along the tuning mode, and σ is the breadth of the coupling function. The coupling strength is $\Lambda=0.18$ eV. The above geometry corresponds roughly to potential energy surfaces of the $S_1(n\pi^*)$ and $S_2(\pi\pi^*)$ excited states of pyrazine[20,68] along the two normal modes ν_{6a} (the tuning mode) and ν_{10a} (the coupling mode). The ground electronic state S_0 of pyrazine lies about 3.94 eV lower than S_1. Here we use a simplified model with the ground state assumed to be S_1 to introduce the effect of the bleach recovery in a general way.

Figure 1 shows diabatic (a) and adiabatic (b) potential surfaces and Fig. 2 shows a close view of the conical intersection in the adiabatic representation, as well as the diabatic coupling, given by Eq. (25). The diabatic surfaces cross along the line [$(n-1)$-dimensional seam], while in an adiabatic representation, the potentials touch at a single point $(Q_{\mathrm{CI}},0)$.

The influence of the bath on the primary system is characterized by the spectral density function $J_\alpha(\epsilon)$. For an Ohmic bath the damping rate is frequency independent and the spectral density in the continuum limit is given by

$$J_\alpha(\omega)=\eta_\alpha\omega e^{-\omega/\omega_{\mathrm{cut}}^{\alpha}} \tag{26}$$

for all frequencies ω up to the cutoff frequency ω_{cut}. The coupling strength η_α for the specific mode is given by the ratio of the damping rate γ and the vibrational frequency of this mode $\omega_{0/c}$. A finite bath with equally spaced sampling of the energy range is used in all calculations. The cutoff frequency is set to $2.5\omega_{0/c}$, which defines the shortest time scale of the bath (about $\tau_{\mathrm{bath}}=20$ fs). The time scale corresponding to the frequency spacing $\Delta\omega$ defines the Poincaré period (τ_{rec}). It should be larger than any other time scale of interest. With ω_{cut} fixed, this time becomes

$$\tau_{\mathrm{rec}}=\frac{2\pi}{\Delta\omega}=\frac{2\pi N}{\omega_{\mathrm{cut}}}. \tag{27}$$

Thus, with an increasing number of bath modes, the convergence progresses in time. In the present modeling the number of TLS is chosen to be $N=30-40$ (for different coupling strengths), which ensures that τ_{rec} is greater than the overall simulation time. The calculations were performed in different interaction regimes identified by considering the relevant time scales: the weak coupling referring to $\gamma^{-1}=750$ fs $\gg\tau_{\mathrm{osc}},\tau_{\mathrm{bath}}$; and the intermediate situation characterized by $\gamma^{-1}=75$ fs $\approx\tau_{\mathrm{osc}}>\tau_{\mathrm{bath}}$. The temperature of the bath has been

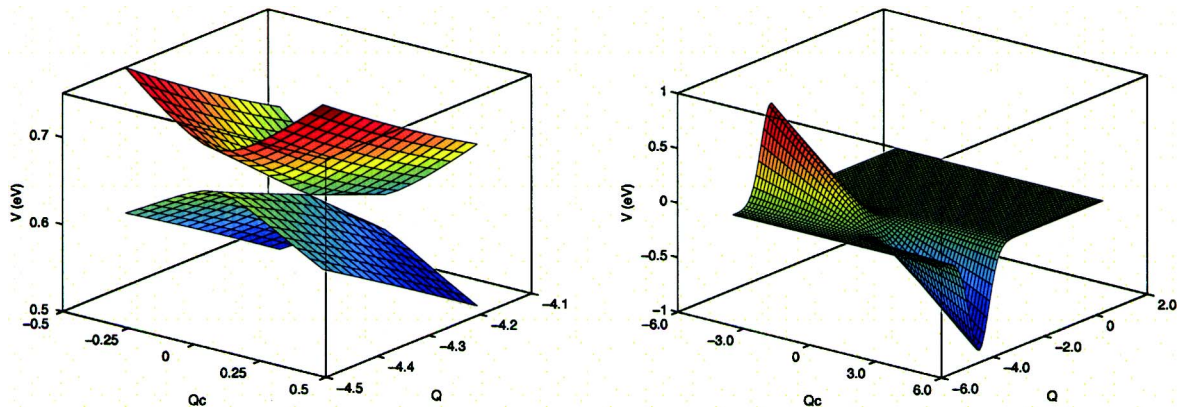

FIG. 2. (Color). (Left) A close view of the conical intersection within the adiabatic representation. (Right) The diabatic coupling V_{d}, giving by Eq. (25).

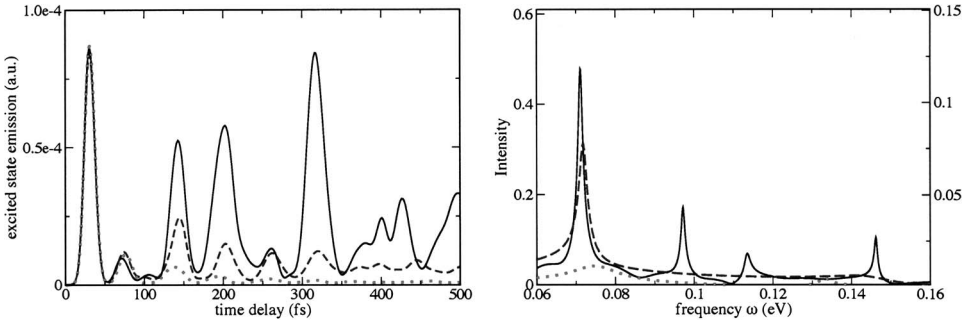

FIG. 3. Transient stimulated-emission signal (left) and its spectrum (right) for the two-mode system, incorporating a conical intersection. The pump and probe frequencies are chosen to correspond to vertical excitation from the bottom of the ground electronic potential. Solid lines: the isolated system; dashed lines: vibrational relaxation with weak system-bath coupling ($\eta_0=\eta_c=0.01$, $\gamma^{-1}=750$ fs); dotted lines: vibrational relaxation ($\eta_0=\eta_c=0.01$) with medium electronic dephasing ($\bar{c}_e=0.25$). The number of bath modes is $N=30$ with two simultaneous excitations allowed. Note the different scale for the spectrum of the isolated system (left ordinate in right panel).

neglected in these calculations and chosen to be zero.

The pump pulse envelope is modeled as a Gaussian function of Eq. (18) with the intensity ϵ_0 adjusted such that approximately 10% of the ground state population was transferred to the excited state.[60] The width (full width at half-maximum) of the pulse which is connected to σ_L is chosen as 20 fs which is typical for charge transfer experiments.[30] $t_{\max}$ is fixed by starting the propagation at $t_0=t_{\max}-3\sigma_L$. The probe pulse has the same profile as the pump pulse, but with only 10% of the pump intensity.

B. Simulation of pump-probe experiment

A direct signature of the ultrafast dynamics is provided by transient modulations of optical observables. In the case of the system with two electronic states, the absorption of the probe pulse reflects the dynamics of the ground state, while the stimulated emission signal reveals the dynamics of the excited state. The transient absorption and emission signals and their spectra are displayed in Figs. 3 and 4. The emission and absorption signals are plotted as a function of the time delay between the pump and probe pulses. The central frequency of the probe pulse is chosen to be the same as of the pump pulse ω_L. The dynamics of the isolated system ($\eta=0$) are compared to those with weak vibrational relaxation ($\eta_0=\eta_c=0.01$, $\gamma^{-1}=750$ fs) and medium electronic dephasing ($\bar{c}_e=0.25$). It was found that pure nuclear dephasing does not affect noticeably the system dynamics on this time scale.

1. Transient emission

The excited state dynamics are reflected by the transient emission of the probe pulse (see the left panel of Fig. 3). After applying the pump pulse of 20 fs duration, about ~10% of the ground state population has been transferred to the electronic excited state. The excited wave packet starts to evolve and eventually reaches the vicinity of the conical intersection. A nonadiabatic population transfer to the ground state takes place within one vibrational period, which is seen as an initial ultrafast decay of the emission signal (~50 fs). The signal for the isolated system (full line) also shows quasiperiodic revivals caused by the nonadiabatic transfer back (recrossings) to the excited potential state. The coherent motions of the excited wave packet are reflected in the periodic oscillations of the signal.

In the presence of vibrational relaxation (dashed line in Fig. 3), the amplitude of the revivals drops down significantly already after 100 fs. However, the initial peak of the emission signal is almost unaffected by the dissipation. In the medium or strong coupling regimes (not shown), the amplitude of the first peak decreases, while the time of its decay (~50 fs) remains unchanged. The influence of electronic dephasing (the dotted line in Fig. 3) is even more pronounced. Hence the emission signal does not show any quasiperiodic recurrences, caused by the population transfer back to the excited state. The periodic oscillations are almost damped down after 300 fs.

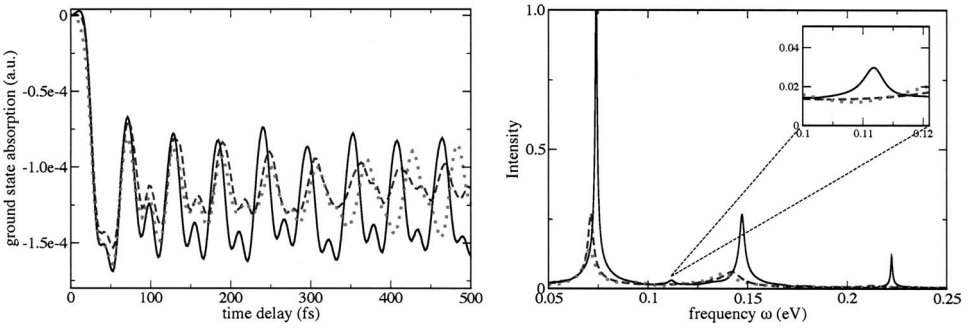

FIG. 4. Transient absorption signal (left) and its spectrum (right) for the two-mode system, involving conical intersection. The pump and probe frequencies are chosen to correspond to the bottom of the ground electronic potential. Solid lines: the isolated system; dashed lines: vibrational relaxation with weak system-bath coupling ($\eta_0=\eta_c=0.01$, $\gamma^{-1}=750$ fs); dotted lines: vibrational relaxation ($\eta_0=\eta_c=0.01$) with medium electronic dephasing ($\bar{c}_e=0.25$). The number of bath modes is $N=30$ and two simultaneous excitations are allowed in the surrogate bath.

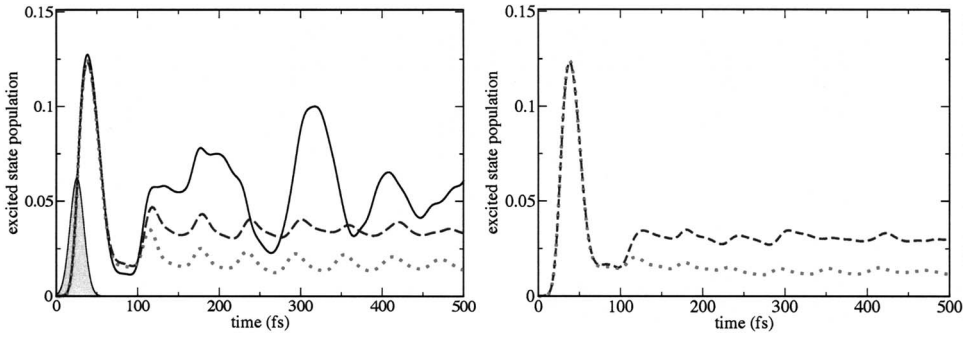

FIG. 5. Time evolution of diabatic (left) and adiabatic (right) population probability of the excited electronic state. Gaussian laser pulse of $\tau_p=20$ fs duration and $\omega_L=1.25$ eV frequency is applied (the envelope of the pulse is shown). Full line: the isolated system ($\eta=0$); dashed line: vibrational relaxation with weak coupling strength ($\eta_0=\eta_c=0.01$, $\gamma^{-1}=750$ fs); dotted line: weak vibrational relaxation ($\eta_0=\eta_c=0.01$) and medium electronic dephasing ($\bar{c}_e=0.25$). The number of bath modes is $N=30$ and two simultaneous excitations are allowed.

Following the dynamics, it is found that the vibrational relaxation and the electronic dephasing effectively obstruct the recrossings of the population to the excited state. As a result the emission signal turns off. The dissipation also damps the coherent motion of the excited wave packet, seen as an increase in the width of the spectrum of the signal.

The spectrum of the emission signal (Fig. 3, right) was obtained by using a filter-diagonalization method[69–71] with a data window between 100 and 450 fs. For the isolated system (full line) it shows the first and second harmonics of the tuning mode Q_0 as well as the fundamental of the coupling mode Q_c. The latter indicates that during the internal-conversion process the coupling mode becomes highly excited. These phenomena reflect the strong mixing induced by the conical intersection. Vibrational relaxation and electronic dephasing reduce the emission signal significantly (note the different scale in Fig. 3, right panel), by suppressing the recrossing process. Furthermore, vibrational relaxation leads to a finite width of the peaks, which increases with increasing system-bath coupling. The bath also red shifts the spectrum. Electronic dephasing causes a further broadening of the peaks and an additional red shift. It also diminishes completely the amplitude of the fundamental frequency of the coupling mode.

2. Transient absorption

The absorption of the probe (Fig. 4, left) reflects the dynamics of the ground electronic state. The transient absorption signal is calculated as the absorption of the probe without the pump pulse subtracted from the absorption of the probe with the pump. The initial decay of the absorption transient (bleach) reveals the loss of ground state population due to the pump pulse. Since the pump pulse excites $\sim 10\%$ of the ground state population to the excited state, the ground state wave packet is only weakly perturbed by the excitation process. However, the "hole" left on the ground electronic state creates a nonstationary density which oscillates periodically with the ground state vibrational frequency.[61,72] These dynamics can be measured experimentally via impulsive resonance Raman scattering. The absorption signal for the isolated system (full line) shows primarily the coherent motion of the remaining ground state wavepacket.

The power spectrum of the absorption signal is given in the right panel of Fig. 4. It shows the first, the second, and higher harmonics of the symmetric mode Q_0 as well as the weak fundamental of the coupling mode Q_c. Since the pump frequency corresponds to the center of the ground electronic potential, the dynamical hole in coordinate space is produced with reflection symmetry with respect to the minimum point of the potential well. A momentum kick induced by the pump will break this symmetry leading to the appearance of a first harmonic component in the signal.[60] In the presence of dissipation, the fundamental of the coupling mode vanishes, while the harmonics of the symmetric mode are diminished significantly. The vibrational relaxation suppresses the higher harmonics faster. Electronic dephasing diffuses the localization of the hole, causing the peak broadening.

After the excited state wave packet has reached the conical intersection, population is nonadiabatically transferred back to the ground state. Therefore the transient absorption of the probe pulse from the ground state should reflect the increase in population, known experimentally as the "recovery of the bleach."[30] The newly created population on the ground electronic surface is vibrationally excited and its appearance in the observation window of the probe is delayed by the time scale of vibrational relaxation. The "recovery of the bleach" phenomenon is governed not only by the population dynamics, which indeed happens on subpicosecond time scale, but also by the energy redistribution. The system must return to the starting configuration for bleach recovery to be observed. The present model shows that even for moderate vibrational relaxation, no "recovery of the bleach" is observed on the time scale shorter than 500 fs.

3. Population probabilities

It is interesting to compare the pump-probe signals to the time evolution of the population probabilities of electronic states. These probabilities have been widely considered as an appropriate measure of nonadiabatic dynamics in systems involving conical intersections.[14,15,64–67]

The time evolution of the *diabatic* population of the excited state is shown in Fig. 5 (left panel). The full lines refer to the dynamics of the isolated system. It exhibits ultrafast decay on a time scale of about 20 fs after the pump pulse has been completed. The population has dropped below 0.02

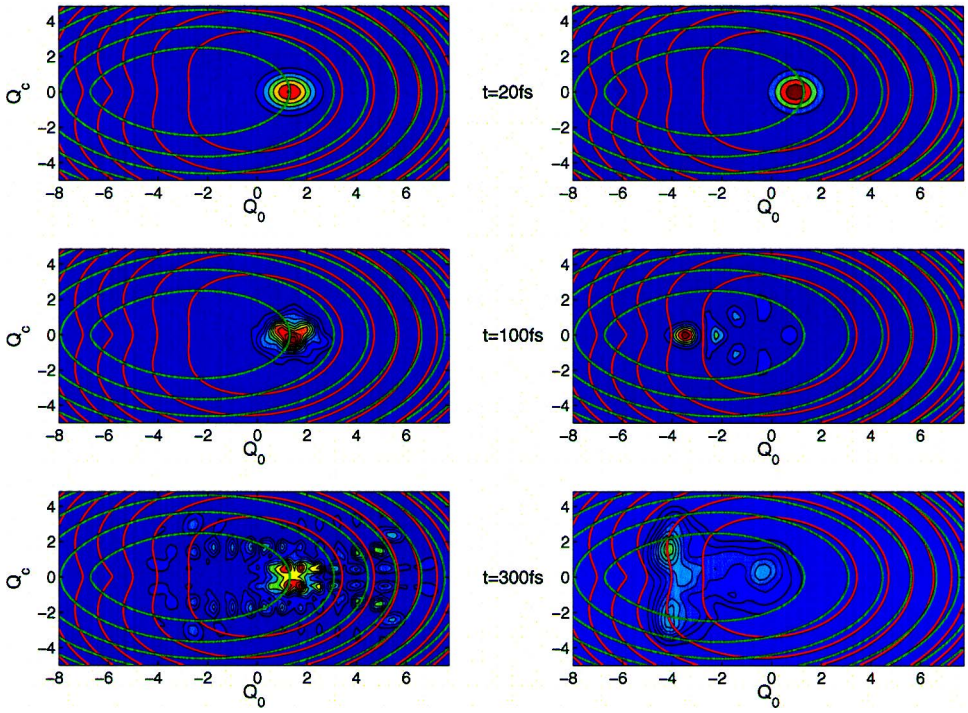

FIG. 6. (Color). The diagonal elements ($Q_n=Q_n'$) of the reduced density matrices in the vibrational coordinate representation $\hat{\boldsymbol{\rho}}_S(Q_0,Q_c;Q_0',Q_c')$ in the adiabatic excited (left panel) and ground (right panel) states. Snapshots are shown at 20 fs (top), 100 fs (middle), and 300 fs (bottom). The red contour lines refer to the adiabatic ground state, while the green contour lines represent the excited state.

(note that only ~10% of the ground state population has been transferred by the pump pulse). This initial decay is followed by pronounced quasiperiodic revivals and the population does not decrease any longer.

Similar behaviors have been obtained for a large variety of multidimensional systems involving conical intersections,[15,23,73–75] including the model with an explicit treatment of the intramolecular environment.[20] All these studies use a Franck–Condon excitation initial state, while the present study starts from an equilibrium initial state and the excitation is caused by the ultrafast pulse. For this reason direct comparison is not possible, nevertheless the time scale of population dynamics is of the same order.

The addition of weak ($\eta_0=\eta_c=0.01$) vibrational relaxation (dashed line in Fig. 5) lowers the amplitude of the revivals and reduces the population in the excited electronic state. In the presence of pure electronic dephasing (dotted lines in Fig. 5) the amplitude of the revivals drops down even more significantly. Neither vibrational relaxation nor pure electronic dephasing changes the rate of the initial interstate crossing, meaning that the ultrafast time scale of the electronic population decay is a feature of the system topology, and is only slightly perturbed by the dissipative environment.[23]

The time evolution of the adiabatic population of the excited state is shown in Fig. 5 (right panel). While the differences from the adiabatic picture are minor, in the long-time limit the population decays to a value slightly lower than in the diabatic picture.

The additional decay in the population probability of the excited state (after 100 fs), caused by the coupling to the environment, indeed reflects the fact that high vibrational levels of the electronic ground state are populated in the initial internal-conversion process.[23,76] Vibrational relaxation cools down this population, and together with electronic dephasing prevents an efficient transfer of the population back to the excited state. However, further energy relaxation to lower vibrational levels of the ground state continues on a much longer time scale. The system's returning to its initial configuration, which can be seen experimentally as recovery of the bleach, is not reflected in the early time evolution of the population probabilities.

Figure 6 displays the diagonal elements ($Q_n=Q_n'$) of the reduced density matrix in the vibrational coordinate representation $\hat{\boldsymbol{\rho}}_S(Q_0,Q_c;Q_0',Q_c')$ (in the diabatic electronic representation). It shows the fast disappearance of the excited wave packet via the conical intersection, and its reappearance in high vibrational levels of the lower surface.

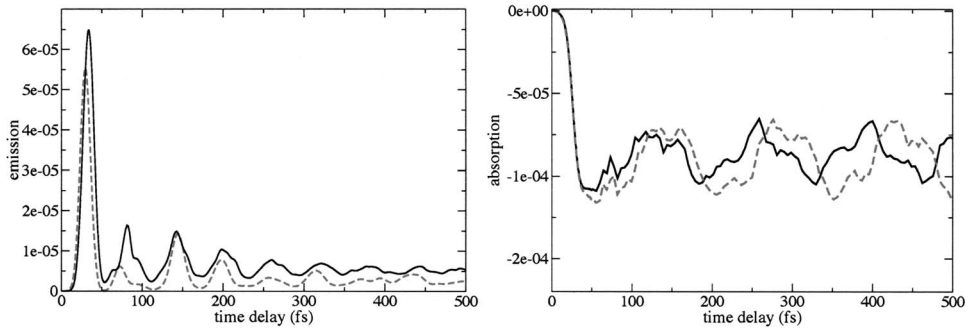

FIG. 7. The stimulated emission (left) and the transient absorption (right) signals for the two-mode system, containing a conical intersection, are calculated using the surrogate Hamiltonian (dashed lines) and the semigroup approaches (solid lines). The vibrational relaxation parameters are in the weak system-bath coupling range ($\eta_0=\eta_c=0.01$, $\gamma^{-1}=750$ fs).

The time evolution of the diabatic state population as well as transient modulations of optical observables are indeed affected by the conical intersection. The population probabilities, however, do not reflect the energy redistribution process and the experimentally measured recovery of the bleach.

C. The surrogate Hamiltonian method versus the semigroup approach

The qualitative features of semigroup dynamics compare well to the surrogate Hamiltonian approach, as can be seen in Fig. 7. For short time dynamics in the weak coupling limit, the two approaches should converge.[42] The difference between the two methods lies in the initial correlation and the influence of the excitation pulse on the system-bath coupling.

The construction of the surrogate Hamiltonian approach is non-Markovian and therefore it is preferable for treatment of ultrashort dynamics at conical intersections. However, in the present study the non-Markovian character of the system-bath interactions hardly affects the dynamics of any of the system's observables. Since the results produced by two methods are qualitatively the same, the Lindblad dynamics proves to be a good approximation.

In the surrogate Hamiltonian calculations the temperature of the bath has been taken to zero, while in the semigroup approach it is set to a finite (low) value to avoid singularities in the relaxation terms D_{ij}. The temperature effects are negligible in the studied system, due to the large excess of energy coming from the electronic excitation.

For short simulation times the surrogate Hamiltonian method is advantageous. For example for simulations up to 500 fsec 40 bath modes were sufficient to obtain the converged results. The wavepacket calculation was faster than the equivalent density operator propagation. In addition the surrogate Hamiltonian method treats the excitation process more realistically since it includes implicitly the influence of the external field on the system-bath coupling. For longer times the computational effort of the surrogate Hamiltonian can become prohibitively expensive due to exponential scaling. The semigroup approach is able to simulate long time dynamics with linear scaling with time. This suggest combining the two methods. In this case the simulation starts using the surrogate Hamiltonian with a fully correlated system-bath initial state. The surrogate Hamiltonian is also used for the pump step, therefore the influence of the field is included. After the pump a reduced system density operator is calculated. This is done by tracing over the bath degrees of freedom from the projection defined by the surrogate Hamiltonian wavefunction $\hat{\boldsymbol{\rho}}_S = \mathrm{tr}_B\{|\Psi\rangle\langle\Psi|\}$. This density operator is used as an initial state for a Liouville dynamics simulation, which can be carried out to longer times.

The above procedure was employed to calculate the recovery of the bleach. The time scale, required to propagate the system to achieve full bleach recovery is in the order of a few picoseconds. Figure 8 shows a monotonic recovery of the bleach on the picosecond time scale obtained from the combined approach.

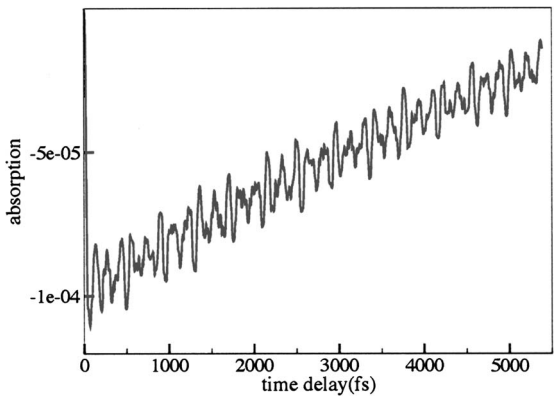

FIG. 8. The recovery of the bleach: a long time simulation of the transient absorption for the two-mode system with a conical intersection. The surrogate Hamiltonian is employed to simulate the system's interaction with the pump pulse used to initiate the dynamics. The system reduced density operator was calculated at the end of the pump pulse and then used as an initial state for the rest of the simulation using the semigroup approach. The parameters of the vibrational relaxation are in the range of medium system-bath coupling ($\gamma^{-1}=500$ fs).

D. Diabatic coupling geometry

It is well documented that nonadiabatic transfer events are extremely sensitive to the landscape of the potentials involved as well as to the nonadiabatic coupling functions.[77] Influence of the dimensionality on nonadiabatic dynamics has been widely discussed.[6,12,14,16] In the context of conical intersections, the issue of the topology also includes a comparison of a true crossing case versus an avoided one, as well as the influence of the form of the diabatic coupling. Studies carried out with slightly anharmonic potentials show the same qualitative behavior.[78]

In many calculations the interstate coupling amplitude is chosen as a constant. A better choice is to localize it near the region of the conical intersection point according to Eq. (25). Figure 9 shows a short-time evolution of the excited state population for the global diabatic coupling $V_d(\hat{\mathbf{Q}}_c)=\Lambda\hat{\mathbf{Q}}_c$ and the localized one [cf. Eq. (25)]. With the global coupling, the excited state is already populated before the excitation. Furthermore, the coupling immediately induces population transfer between the excited and the ground states. This is

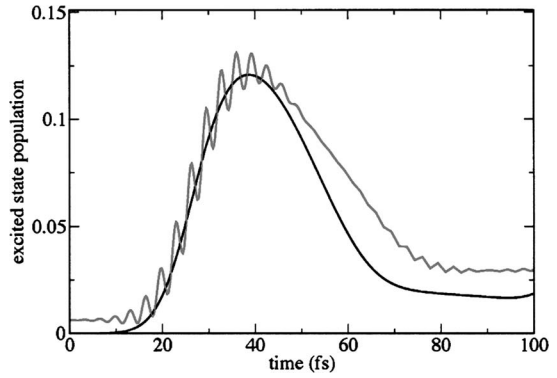

FIG. 9. The population of the excited state for global ($V_d=\Lambda Q_c$) and local ($V_d=\Lambda Q_c e^{-(Q_0-Q_{CI})^2/\sigma^2-Q_c^2/\sigma^2}$) diabatic couplings. Short time dynamics is shown in the presence of weak vibrational coupling ($\eta_0=\eta_c=0.01$, $\gamma^{-1}=750$ fs).

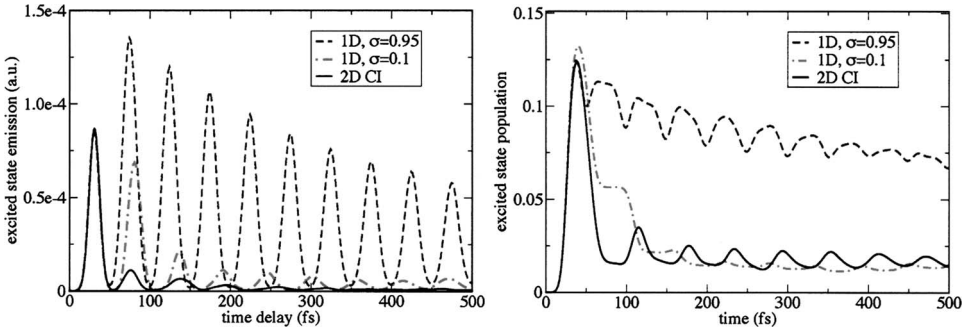

FIG. 10. The nonadiabatic dissipative dynamics of a two-dimensional system, involving a conical intersection (full lines) versus a one-dimensional system with a local (σ=0.95) nonadiabatic coupling (dashed lines). Dashed-dotted lines: a one-dimensional system with more localized coupling (σ=0.1). The transient stimulated-emission signal (left) and the population probability of the excited state (right) are shown. The strength of the diabatic coupling is Λ =0.18 eV for all cases. The calculations are made for the system with weak vibrational relaxation ($\eta_0=\eta_c=0.01$) and medium electronic dephasing ($\bar{c}_e$ =0.25).

seen as fast oscillations with a frequency proportional to the electronic excitation energy 2Δ. As the diabatic coupling becomes more localized, one can observe a turnover effect.[79] First, the initial decay of the excited state population becomes more pronounced and then for very localized coupling the population is trapped in the excited state. This behavior is similar to the turnover effect as a function of the coupling constant Λ. The effect of the damping is less profound for the systems with a conical intersection compared with the one-dimensional nonadiabatic systems.[36]

Next we compare the nonadiabatic dynamics of the two-dimensional (2D) system, involving a conical intersection, and those of the 1D system with a local diabatic coupling. The parameters of the 1D system are chosen to be the same as the tuning mode's geometry in the 2D model (ω_0=0.074, κ_g=−0.0964, κ_e=0.1194, Δ=0.4617, all in eV). The diabatic coupling potential has a form of a damped Gaussian:

$$V_{\mathrm{d}}(\hat{\mathbf{Q}}) = \Lambda e^{-(\hat{\mathbf{Q}} - Q^*)^2/2\sigma^2}, \tag{28}$$

with Q^* being the position of the maximum coupling (referring to the point where the conical intersection occurs along the tuning mode in the 2D model). The same strength of the coupling (Λ=0.18 eV) has been chosen for the both systems.

Figure 10 displays the transient stimulated emission as a function of the time delay (left) and the time evolution of the diabatic population probability of the excited state (right) for two systems. The nonadiabatic dynamics are shown in the presence of dissipation (both vibrational relaxation and electronic dephasing are included). An initial fast decay of the excited state's population, typical for the system incorporating a conical intersection, does not occur in the 1D system. There, the population, as well as the stimulated emission signal, exhibit much slower decay. The dynamics can be accelerated by further localizing of the diabatic coupling, but the turnover will eventually stop an additional increase in the decay rate.

Next we compare the nonadiabatic dynamics for the two-state two-mode system with different forms of the diabatic couplings. Figure 11 shows the stimulated-emission signal (left) and the dynamics of the population probabilities (right) for three models. The dynamics of the system with a conical intersection (a true crossing) is compared to the system which involves an avoided surface crossing. In the avoided crossing model the diabatic coupling does not depend on the Q_c coordinate and is represented by a damped Gaussian according to Eq. (28). The third model has a symmetric diabatic coupling:

$$V_{\mathrm{d}}(\hat{\mathbf{Q}}_0, \hat{\mathbf{Q}}_c) = \Lambda |\hat{\mathbf{Q}}_c| e^{(\hat{\mathbf{Q}}_0 - Q_{\mathrm{CI}})^2/2\sigma^2}. \tag{29}$$

The dynamics of the population in the system with the avoided crossing are qualitatively similar to the dynamics in the 1D model (Fig. 10). The decay is slower than in the crossing model. The oscillations of the stimulated-emission

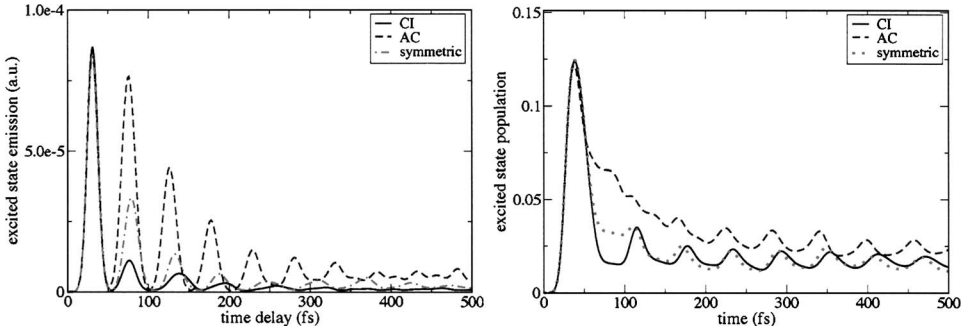

FIG. 11. The nonadiabatic dissipative dynamics of a system with (a) a conical intersection (full lines), (b) an avoided crossing (dashed lines), and (c) a symmetric coupling (dashed-dotted lines). The transient stimulated-emission (left) and the population probability of the excited state (right) are shown for the system in presence of weak vibrational relaxation ($\eta_0=\eta_c=0.01$) and electronic dephasing ($\bar{c}_e$=0.25). The strength of the diabatic coupling is Λ=0.18 eV for all cases.

signal, indicating the coherent motion of the excited wave packet, persist for quite a long time (more than 500 fs). If the diabatic coupling is symmetric, the adiabatic surfaces exhibit a true crossing. The coupling, however, does not change a sign at the crossing point $(Q_{\mathrm{CI}},0)$. In this case the stimulated-emission exhibits a fast decay, which is nevertheless slower than one for the system with a conical intersection. Only for the true conical intersection does the highly localized diabatic coupling cause the fastest initial decay of the observables associated with the excited state population.

IV. CONCLUSIONS

The present study elucidates the dynamics of a system incorporating a conical intersection in the presence of a dissipative environment. The system was described by a model consisting of two vibronically coupled electronic states and two nuclear degrees of freedom. Dissipation is treated by using the surrogate Hamiltonian approach and a reduced density operator dynamics based on the Lindblad formalism. The use of the surrogate Hamiltonian has the advantage of a consistent treatment of initial correlations, non-Markovian dynamics, and an explicit description of the pulse field. The latter is of a special importance, since our study is aimed at time-dependent observables, which can be directly related to experiments.

Widely discussed adiabatic electronic state populations can only be partially connected to experimental pump-probe signals. Therefore the present study emphasizes the transient modulations of optical observables, which are a direct signature of the ultrafast dynamics, measured in the pump-probe experiments. The nonperturbative approach has been employed for describing the dynamics induced by the pump pulse, while the weak probe has been treated within a perturbative picture. This allows us to associate a quantum mechanical window operator to the absorption of the probe pulse centered at time t. The stimulated emission and absorption have been calculated as expectation values of this window operator.

The stimulated emission signals show a rapid initial decay on a time scale of tens of femtoseconds, which can be associated with an ultrafast nonadiabatic transition via a conical intersection. This initial decay is almost unaffected by vibrational relaxation and the electronic dephasing. The dissipation becomes important in the following stage: it prevents a back transfer (recrossing) leading to a subpicosecond relaxation of the excited state population.

At the same time, it is clear that the pump-probe spectra are governed not only by the population dynamics, but also by the energy redistribution. After the initial curve crossing, the system may return close to its initial prepump configuration. Experimentally this is associated with the recovery of the bleach observed in the transient absorption signal. The *ground* state recovery dynamics, i.e., the bleach recovery and the cooling of the hot vibrational population, are not reflected in the electronic population probabilities. In our model the absorption signal shows coherent oscillations of the slightly perturbed ground state wave packet and apparently no fast recovery of the bleach up to 500 fsec. We can conclude that the energy relaxation, dominated by an intramolecular vibrational relaxation, proceeds much more slowly. The origin of the fast bleach recovery, measured in charge-transfer experiments[29–31] remains unclear, but might well arise from simple avoided crossing with a sufficiently strong local diabatic coupling and efficient IVR.

ACKNOWLEDGMENTS

This research was partly supported by the Israel Science Foundation ISF. The Fritz Haber Center is supported by the Minerva Gesellschaft für die Forschung, GmbH München, Germany. M.R. thanks the Chemistry Division of the NSF for support of this work. We are grateful to W. Domcke, J. Michl, and T. Martinez for helpful comments.

[1] M. Born and J. R. Oppenheimer, Ann. Phys. (Leipzig) **87**, 457 (1927).
[2] A. Nitzan and J. Jortner, J. Chem. Phys. **56**, 5200 (1972).
[3] R. Longo, E. Deumens, A. Diz, and Y. Ohrn, Rev. Mod. Phys. **66**, 917 (1994).
[4] L. D. Landau, Phys. Z. Sowjetunion **2**, 46 (1932).
[5] C. Zener, Proc. R. Soc. London, Ser. A **137**, 696 (1932).
[6] H. Nakamura, *Nonadiabatic Transition* (World, River Edge, 2002).
[7] M. Baer, Adv. Chem. Phys. **124**, 39 (2002).
[8] M. Bixon and J. Jortner, Adv. Chem. Phys. **106**, 35 (1999).
[9] J. von Neumann and E. Wigner, Phys. Z. **30**, 467 (1929).
[10] E. Teller, J. Phys. Chem. **41**, 109 (1937).
[11] F. Bernardi, S. De, M. Olivucci, and M. A. Robb, J. Am. Chem. Soc. **112**, 1737 (1990).
[12] J. Michl and V. Bonačić-Koutecký, *Electronic Aspects of Organic Photochemistry* (Wiley, New York, 1990).
[13] F. Bernardi, M. Olivucci, and M. A. Robb, Chem. Soc. Rev. **25**, 321 (1996).
[14] *Conical Intersections. Electronic Structure, Dynamics and Spectroscopy*, edited by W. Domcke, D. R. Yarkony, and H. Köppel (World Scientific, Singapore, 2004).
[15] H. Köppel, W. Domcke, and L. S. Cederbaum, Adv. Chem. Phys. **57**, 59 (1984).
[16] G. Stock and W. Domcke, Adv. Chem. Phys. **100**, 1 (1997).
[17] A. Toniolo, G. Granucci, and T. J. Martinez, J. Phys. Chem. A **107**, 3822 (2003).
[18] A. Toniolo, M. Ben-Nun, and T. J. Martinez, J. Phys. Chem. A **107**, 829 (2003).
[19] A. Toniolo, S. Olsen, L. Manohar, and T. J. Martinez, Faraday Discuss. Chem. Soc. **127**, 149 (2004).
[20] G. A. Worth, H.-D. Meyer, and L. S. Cederbaum, J. Chem. Phys. **109**, 3518 (1998).
[21] A. G. Redfield, Phys. Rev. **98**, 1787 (1955).
[22] A. G. Redfield, IBM J. Res. Dev. **1**, 19 (1957).
[23] A. Kühl and W. Domcke, J. Chem. Phys. **116**, 263 (2002).
[24] T. Gerdts and U. Manthe, Chem. Phys. Lett. **295**, 167 (1998).
[25] G. Lindblad, Commun. Math. Phys. **48**, 119 (1976).
[26] V. Gorini, A. Kossokowski, and E. C. G. Sudarshan, J. Math. Phys. **17**, 821 (1976).
[27] R. Alicki and K. Lendi, *Quantum Dynamical Semigroups and Applications* (Springer-Verlag, Berlin, 1987).
[28] R. Baer and R. Kosloff, J. Chem. Phys. **106**, 8862 (1997).
[29] P. F. Barbara, G. C. Walker, and T. P. Smith, Science **256**, 975 (1992).
[30] P. Kambhampati, D. H. Son, T. W. Kee, and P. F. Barbara, J. Phys. Chem. A **104**, 10637 (2000).
[31] P. F. Barbara, P. J. Reid, C. Silva, and J. T. Hupp, J. Phys. Chem. **99**, 2609 (1995).
[32] U. Weiss, *Quantum Dissipative Systems* (World Scientific, Singapore, 1999).
[33] G. Herzberg and H. C. Longuet-Higgins, Faraday Discuss. Chem. Soc. **35**, 77 (1967).
[34] T. Klüner, S. Thiel, and V. Staemmler, J. Phys. B **32**, 4931 (1999).
[35] T. Pacher, L. S. Cederbaum, and H. Köppel, Adv. Chem. Phys. **84**, 293 (1993).
[36] C. P. Koch, T. Klüner, and R. Kosloff, J. Chem. Phys. **116**, 7983 (2002).
[37] A. Ferretti, A. Lami, and G. Villani, J. Chem. Phys. **106**, 934 (1997).

[38] W. H. Louisell, *Quantum Statistical Properties of Radiation* (Wiley, New York, 1990).
[39] N. Makri, J. Phys. Chem. B **103**, 2823 (1999).
[40] N. G. van Kampen, *Stochastic Processes in Physics and Chemistry* (North-Holland, Amsterdam, 1992).
[41] C. P. Koch, T. Klüner, H.-J. Freund, and R. Kosloff, Phys. Rev. Lett. **90**, 117601 (2003).
[42] D. Gelman, C. P. Koch, and R. Kosloff, J. Chem. Phys. **121**, 661 (2004).
[43] R. Kosloff, "The Fourier method," in *Numerical Grid Methods and Their Applications to Schrödinger Equation* (Kluwer Academic, The Netherlands, 1993).
[44] R. Kosloff and H. Tal-Ezer, Chem. Phys. Lett. **127**, 223 (1986).
[45] R. Kosloff, J. Chem. Phys. **92**, 2087 (1988).
[46] D. Kohen, C. C. Martson, and D. Tannor, J. Chem. Phys. **107**, 5236 (1997).
[47] R. Zwanzig, J. Stat. Phys. **9**, 215 (1973).
[48] T. Arimitsu, Y. Takahashi, and F. Shibata, Physica A **100**, 507 (1980).
[49] K. Kraus, Ann. Phys. (N.Y.) **64**, 311 (1971).
[50] G. Katz, R. Kosloff, and M. Ratner, Isr. J. Chem. **44**, 53 (2004).
[51] G. Katz, Y. Zeiri, and R. Kosloff, Chem. Phys. Lett. **358**, 284 (2002).
[52] R. Kosloff, P. Saalfrank, and R. Baer, Chem. Phys. Lett. **230**, 463 (1994).
[53] L. Diosi, Physica A **199**, 517 (1993).
[54] L. Diosi, N. Gisin, and W. T. Struntz, Phys. Rev. A **58**, 1699 (1998).
[55] A. H. Zewail, *Femtochemistry—Ultrafast Dynamics of the Chemical Bond* (World Scientific, Singapore, 1994).
[56] R. W. Schoenlein, L. A. Peteanu, R. A. Mathies, and C. V. Shank, Science **254**, 412 (1991).
[57] N. H. Damrauer, G. Cerullo, A. Yeh, T. R. Boussie, C. V. Shank, and J. K. McCusker, Science **275**, 54 (1997).
[58] A. T. Yeh, C. V. Shank, and J. K. McCusker, Science **289**, 235 (2000).
[59] Q. Wang, R. W. Schoenlein, L. A. Peteanu, R. A. Mathies, and C. V. Shank, Science **266**, 5184 (1994).
[60] E. Gershgoren, J. Vala, R. Kosloff, and S. Ruhman, J. Phys. Chem. A **105**, 5081 (2001).
[61] U. Banin, A. Bartana, S. Ruhman, and R. Kosloff, J. Chem. Phys. **101**, 8461 (1994).
[62] L. W. Ungar and J. A. Cina, Adv. Chem. Phys. **100**, 171 (1997).
[63] N. F. Scherer, R. J. Carlson, A. Matro, M. Du, A. J. Ruggiero, V. Romero-Rochin, J. A. Cina, G. R. Fleming, and S. A. Rice, J. Chem. Phys. **95**, 1487 (1991).
[64] W. Domcke and H. Köppel, Chem. Phys. Lett. **140**, 133 (1987).
[65] G. Stock, R. Schneider, and W. Domcke, J. Chem. Phys. **90**, 7184 (1989).
[66] G. Stock and W. Domcke, Phys. Rev. A **45**, 3032 (1992).
[67] L. Seidner, G. Stock, and W. Domcke, J. Chem. Phys. **103**, 3998 (1995).
[68] R. Schneider, W. Domcke, and H. Köppel, J. Chem. Phys. **92**, 1045 (1990).
[69] M. R. Wall and D. Neuhauser, J. Chem. Phys. **102**, 8011 (1995).
[70] V. A. Mandelshtam and H. S. Taylor, J. Chem. Phys. **107**, 6756 (1997).
[71] V. A. Mandelshtam, J. Chem. Phys. **108**, 9999 (1998).
[72] G. Ashkenazi, R. Kosloff, S. Ruhman, and H. Tal-Ezer, J. Chem. Phys. **103**, 10005 (1995).
[73] H. Köppel, L. S. Cederbaum, and W. Domcke, J. Chem. Phys. **89**, 2023 (1988).
[74] U. Manthe and H. Köppel, J. Chem. Phys. **93**, 345 (1990).
[75] F. Santoro and C. Petrongolo, J. Chem. Phys. **110**, 4419 (1999).
[76] A. Kühl and W. Domcke, Chem. Phys. **259**, 227 (2000).
[77] D. R. Yarkony, J. Chem. Phys. **114**, 2601 (2001).
[78] D. M. Lockwood, M. Ratner, and R. Kosloff, J. Chem. Phys. **117**, 10125 (2002).
[79] G. Ashkenazi, R. Kosloff, and M. A. Ratner, J. Am. Chem. Soc. **121**, 3386 (1999).